Nanoscale Res Lett (2010) 5:1619–1626
DOI 10.1007/s11671-010-9685-z

NANO EXPRESS

# Cation-Induced Coiling of Vanadium Pentoxide Nanobelts

**Jun Liu · Dongfeng Xue**

Received: 8 June 2010 / Accepted: 1 July 2010 / Published online: 11 July 2010


**Abstract** Single-crystalline $V_2O_5 \cdot xH_2O$ nanorings and microloops were chemically assembled via an ion-induced chemical spinning route in the designed hydrothermal system. The morphology and structure of products were investigated by means of scanning electron microscopy (SEM) and transmission electron microscopy (TEM). X-ray powder diffraction (XRD) measurement, energy-dispersive X-ray spectroscopy (EDS) microanalysis and thermal gravimetric analysis (TGA) revealed that the composition of nanorings and microloops is $V_2O_5 \cdot 1 \cdot 1H_2O$. For these oxide nanorings and microloops, the cation-induced coiling growth mechanism of vanadium pentoxide nanobelts has been proposed on the basis of crystallographic structure of vanadium pentoxide. Our proposed chemical spinning process and the rational solution-phase synthesis route can also be extended to prepare novel 1D materials with layered or more complex structures.

**Keywords** $V_2O_5 \cdot xH_2O$ · Nanoring · Ion-induced chemical spinning route · Morphology · Cation-induced coiling · Vanadium pentoxide nanobelts · Solution-phase synthesis route

## Introduction

Control over the composition, shape, spatial location and/or geometrical configuration of functional nanostructures is of importance for nearly all practical applications of these materials [1–6]. One-dimensional (1D) nanostructures such as nanorods, nanowires, nanobelts and nanotubes with high aspect ratios have been attracting much attention lately due to their high potential applications in electronic device fabrications, sensors, etc. [7–15]. Recently, it has been demonstrated that several new geometrical configurations such as nanosprings [16], nanorings[16, 17], and nanohelices [18, 19] grown from 1D nanobelts or nanowires are of special interest owing to their unique periodic and elastic properties resulting in structural flexibility that provides additional opportunities for nanoengineering. The ability to construct artificial ringlike building units has implications in the rational design of complex nanostructures for precise nanofabrication. Although much progress has been made in the synthesis of nanorings by coiling of nanobelts, all these successes are based on materials with polar surfaces [16–19]. Here, we demonstrate a new mechanism of forming nanorings by coiling of nanobelts, i.e., cation-induced asymmetric strain on top and bottom surfaces of nanobelts. Different from previous work based on polar surfaces, our designed strategy can be applied to structures without anion- and cation-terminated surfaces.

As a well-known transition-metal oxide, vanadium pentoxide ($V_2O_5 \cdot xH_2O$, normally, $x$ falls in the range of 0–3) has been extensively studied due to its applications in the field of lithium–ion batteries [20], electric field-effect transistors [21], actuators [22], catalysis [23], and sensors [24]. Various 1D nanostructures of $V_2O_5 \cdot xH_2O$ such as nanorods [25], nanowires [25] and nanotubes [26, 27] have already been synthesized. However, it is a big challenge to rationally design a synthetic route for fabrication of vanadium pentoxide nanorings. In this work, $V_2O_5 \cdot xH_2O$ single-crystalline nanorings and microloops were successfully synthesized in the designed hydrothermal system.

J. Liu · D. Xue (✉)
State Key Laboratory of Fine Chemicals, Department of Materials Science and Chemical Engineering, School of Chemical Engineering, Dalian University of Technology, 116012 Dalian, People's Republic of China
e-mail: dfxue@chem.dlut.edu.cn

## Experimental Details

### Synthesis

$V_2O_5{\cdot}xH_2O$ nanorings and microloops were synthesized in a hydrothermal process. In a typical process, 0.2–0.4 g ammonium metavanadate ($NH_4VO_3$) was dissolved in distilled water (20–40 ml) to form a light yellow clear solution. Then 0.5–1 g magnesium nitrate was added to this solution under vigorous stirring. Afterward, nitric acid (5 mol/l) was added drop-wise under stirring until the final pH of the solution was 3–5. A clear orange solution was formed, which was transferred into a Teflon-lined stainless steel autoclave. The autoclave was sealed and maintained at 160–190°C for 20–40 h. After the solution was cooled to room temperature, the obtained solid products were collected by centrifuging the mixture, which were then washed with absolute ethanol and distilled water several times and dried at 60–80°C for 4–8 h for further characterization. The anhydrous $V_2O_5$ nanostructure was obtained by annealing $V_2O_5{\cdot}xH_2O$ nanorings and microloops in air under atmospheric pressure at 500°C for 2 h.

### Characterization

The collected products were characterized by an X-ray diffraction (XRD) on a Rigaku-DMax 2400 diffractometer equipped with the graphite monochromatized Cu Ka radiation flux at a scanning rate of $0.02°s^{-1}$ in the $2\theta$ range of 5–60°. Scanning electron microscopy (SEM) images were taken with a JEOL-5600LV scanning electron microscope, using an accelerating voltage of 20 kV. Energy-dispersive X-ray spectroscopy (EDS) microanalysis of the samples was performed during SEM measurements. The structure of $V_2O_5{\cdot}xH_2O$ was investigated by transmission electron microscopy (TEM, Philips, TecnaiG2 20, operated at 200 kV). To analyze the water content in the sample, the sample was investigated using a thermogravimetric analyzer (Mettler Toledo TGA/SDTA851e), in flowing $N_2$ and at a heating rate of 10°C/min. UV–Vis adsorption spectra were recorded on UV–Vis–NIR spectrophotometer (JASCO, V-570).

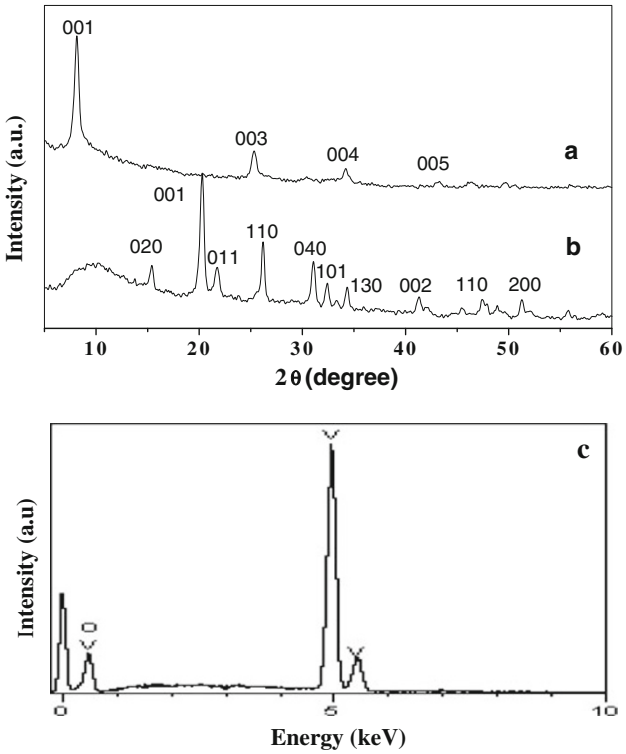


**Fig. 1** XRD patterns of **a** $V_2O_5{\cdot}xH_2O$ nanorings and microloops and **b** anhydrous $V_2O_5$ after annealing at 500°C for 2 h. **c** EDS pattern of the $V_2O_5{\cdot}xH_2O$ nanorings and microloops

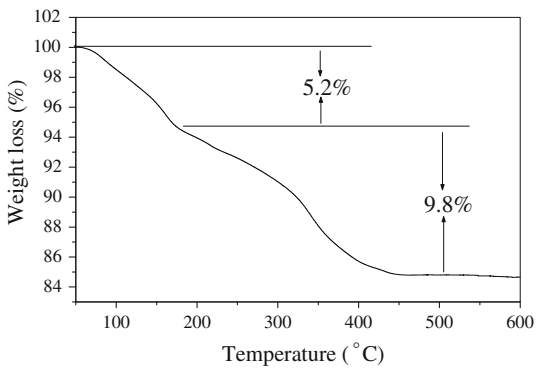


**Fig. 2** TGA curve of the as-synthesized $V_2O_5{\cdot}xH_2O$ nanorings and microloops. XRD, EDS and TGA analyses indicate that the composition of the as-prepared products is $V_2O_5{\cdot}1{\cdot}1H_2O$

## Results and Discussion

Typical XRD pattern of $V_2O_5{\cdot}xH_2O$ nanorings and microloops displays a set of peaks characteristic of (00 *l*) reflections for the layered structure $V_2O_5{\cdot}xH_2O$ (Fig. 1a), which is consistent with the reported data [28]. After calcining the products at 500°C for 2 h, XRD pattern (Fig. 1b) can be indexed as the orthorhombic $V_2O_5$ (space group *Pmm*, $a = 11.516$, $b = 3.566$, $c = 3.777$ Å, JCPDS card no. 41-1426). EDS analysis was also used to determine the chemical composition of an individual $V_2O_5{\cdot}xH_2O$ nanoring and microloop (Fig. 1c). The result shows that these nanorings and microloops contain only V and O elements. In order to analyze the water content in the current sample, TGA was carried out on them in $N_2$. The TGA curve is shown in Fig. 2, which shows the as-obtained sample has two dehydration processes. The TGA plot shows a weight loss of 15% up to 600°C, which is related to the procedure

of dehydration. The weight loss of 5.2% below 200°C can be attributed to the release of water absorbed on the sample, and the weight loss of 9.8% in the range of 160–600°C is believed to correspond to the release of water in the crystals [29]. Based on the XRD pattern, EDS spectrum and TGA analysis, the composition of the as-prepared products is $V_2O_5{\cdot}1{\cdot}1H_2O$.

The morphology and structure of the products was observed by means of SEM and TEM. A low-magnification SEM image shows that dominant components of the as-synthesized products are nanobelts with the length ranging from several tens to several hundred micrometers, but a significant number of nanobelts have ring or loop shape (Fig. 3a). High-magnification SEM images show that there are three types of nanorings and microloops (1) circular rings and microloops (Fig. 3b, c, f, g), (2) trigonal rings and microloops (Fig. 3d, h), and (3) tetragonal rings and microloops (Fig. 3e, i). It can be seen that all these $V_2O_5{\cdot}xH_2O$ nanorings have a perfect shape of complete rings with the smooth and flat surface (more nanorings and microloops are shown in Fig. 4). Detailed observation reveals that the circular nanorings and microloops have a

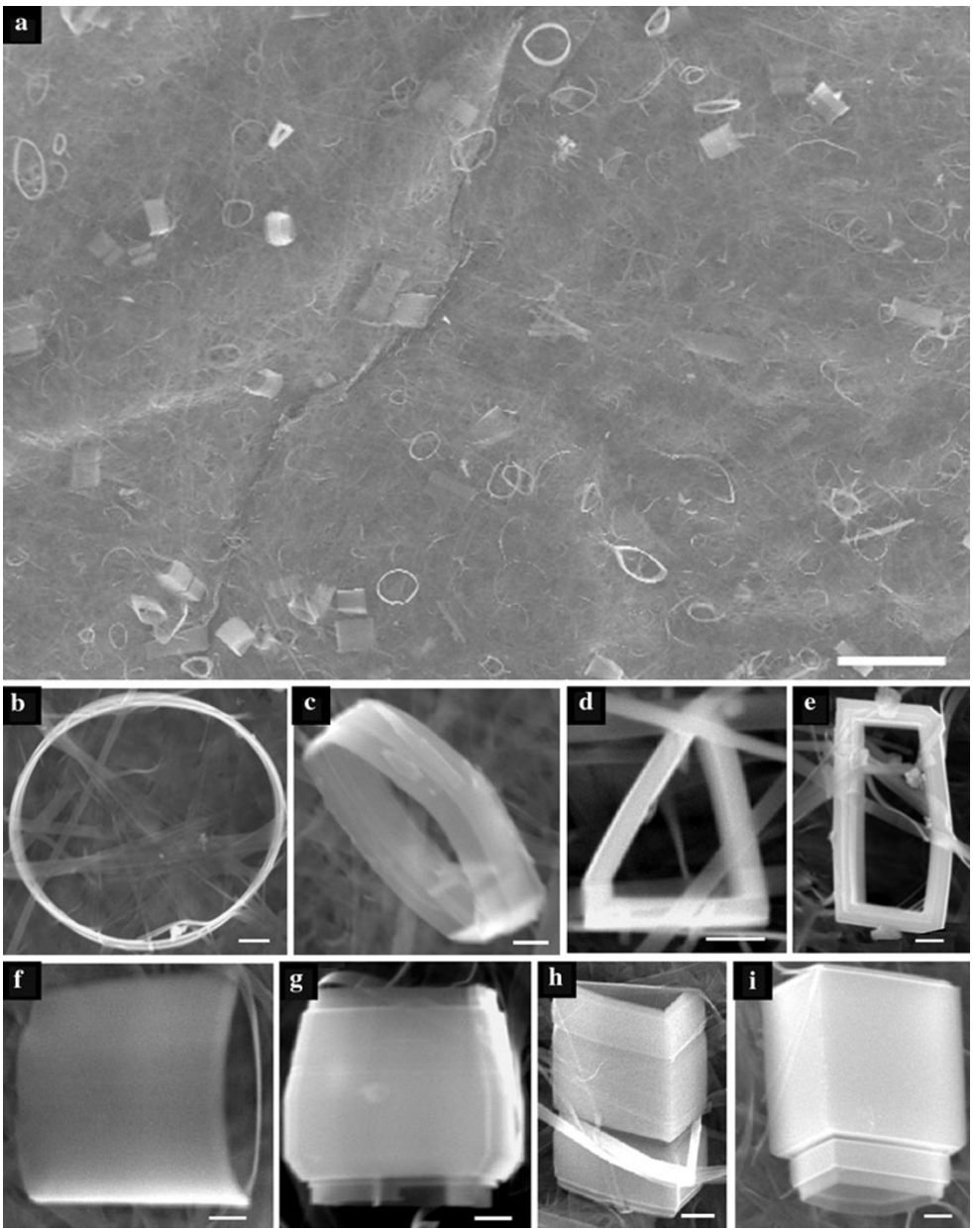


**Fig. 3** Low-magnification SEM image (**a**) and representative high-magnification SEM images (**b–i**) of $V_2O_5{\cdot}xH_2O$ structures. The type (1) circular nanorings and microloops (**b**, **c**, **f**, **g**), the type (2) trigonal nanorings and microloops (**d**, **h**), and the type (3) tetragonal nanorings and microloops (**e**, **i**). *Scale bars* correspond to 20 μm (**a**) and 1 μm (**b–i**)

diameter of 3–10 μm, coiling of nanobelts with the thickness of 20–30 nm and width of 300–500 nm.

TEM and selected-area electron diffraction (SAED) provide further insight into microstructural details of these interesting structures. Figure 5a shows TEM image of one $V_2O_5{\cdot}xH_2O$ single-crystalline nanoring with a diameter of about 3 μm. The corresponding SAED pattern shown in the inset shows the single-crystalline nature of the whole nanoring. Figure 5b is an enlargement of area marked in Fig. 5a, which clearly shows the complete nanoring is made by coiling of single-crystalline nanobelts. A high-resolution TEM image shows that the nanoring is single crystalline (Fig. 5c). The measured lattice shows that the resolved interplanar distance $d = 2.1$ Å can be determined as the [010] growth direction of these nanobelts [30].

For the synthesis of inorganic nanorings by coiling of nanobelts, a polar surface–driven kinetic model has ever been proposed [16–19], and geometrically, the cation- and anion-terminated surfaces are the characteristic structure of these target compounds. To minimize the electrostatic interaction energy among the polar charges, the nanobelt dominated by polar surfaces tends to fold over, resulting in the formation of single-crystalline nanorings. Different from the previous work, the as-synthesized $V_2O_5{\cdot}xH_2O$ is a layered structure material without a pair of positively and negatively charged polar surfaces in our process. The

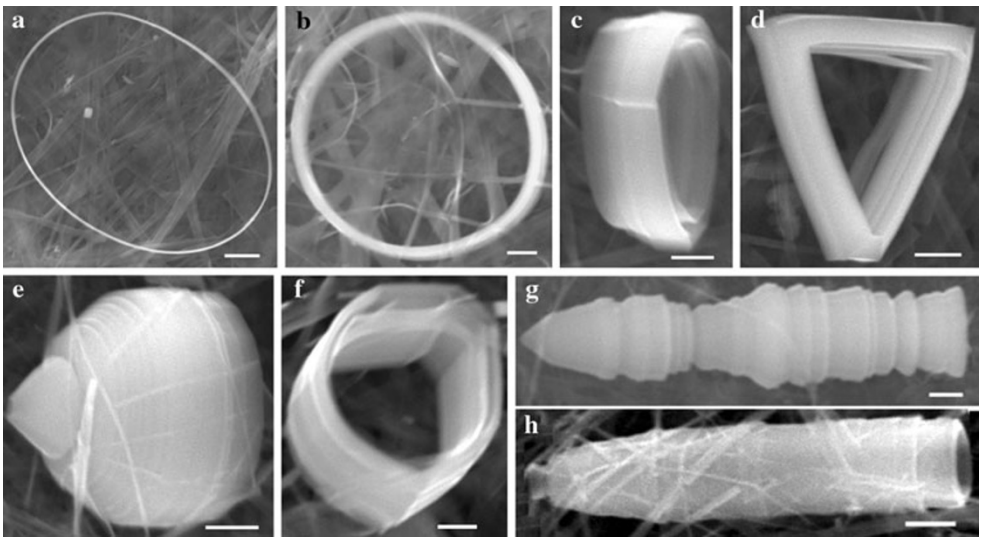


**Fig. 4** SEM images of the as-systhesized $V_2O_5{\cdot}xH_2O$ nanorings and microloops. *Scale bars* correspond to 1 μm

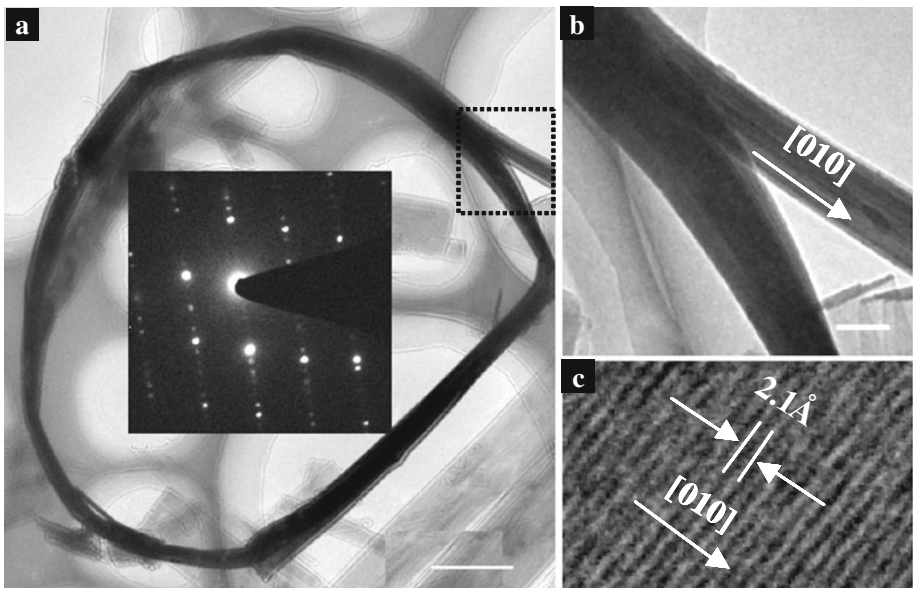


**Fig. 5** TEM characterizations of $V_2O_5{\cdot}xH_2O$ nanorings. **a** TEM image of a single $V_2O_5{\cdot}xH_2O$ nanoring. The *inset* is SAED pattern of a nanoring indicating the single-crystalline nature of the whole nanoring. **b** Enlargement of area marked in **a** showing the coiling of nanobelt to form the nanoring. **c** HRTEM image taken from a $V_2O_5{\cdot}xH_2O$ nanoring. *Scale bars* correspond to 500 nm (**a**) and 100 nm (**b**)

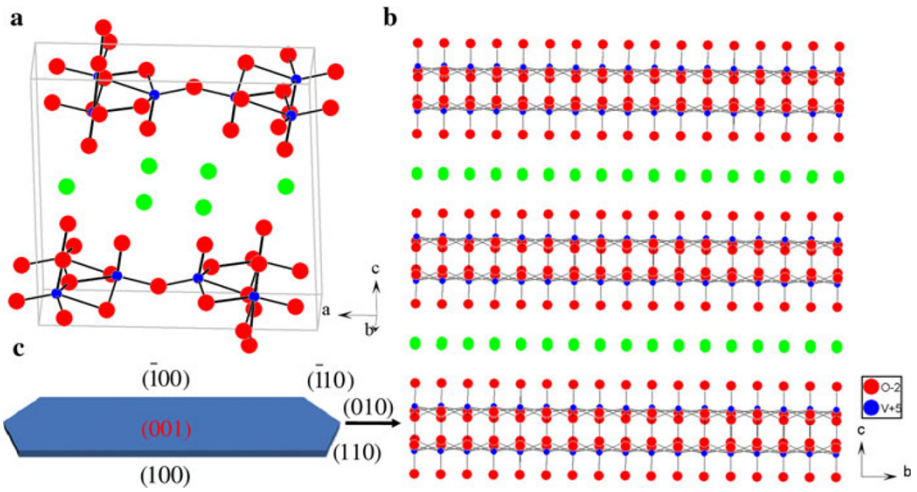


**Fig. 6** Crystal structure and simulated morphology of $V_2O_5{\cdot}xH_2O$. **a** Monoclinic structure model of $V_2O_5{\cdot}xH_2O$. **b** The structure model of $V_2O_5{\cdot}xH_2O$ projected along [100] direction or *a*-axis, displaying the structure of stacking bilayers of single $V_2O_5$ layer along *c*-axis. Water molecules are shown in green. **c** Simulated thermodynamic equilibrium morphology of $V_2O_5{\cdot}xH_2O$ via the chemical bonding theory of single crystal growth

structure of $V_2O_5{\cdot}xH_2O$ can be well described as stacking of well-defined bilayers of single $V_2O_5$ layer made of squarepyramidal $VO_5$ units with water molecules residing between them along its *c*-axis (Fig. 6a) [28]. By projecting the structure model along the [100] direction, the ± (001) planes are terminated solely with negative $O^{2-}$ (Fig. 6b).

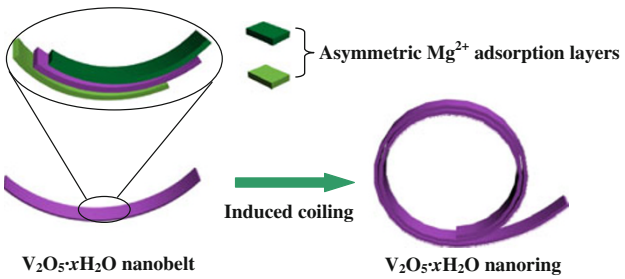


**Fig. 7** Schematic illustration of the formation process of $V_2O_5{\cdot}xH_2O$ nanorings by $Mg^{2+}$-induced asymmetric strain of nanobelts

The driven force for nanorings and microloops formation in our designed process is $Mg^{2+}$-induced asymmetric strain on the top and bottom surfaces of $V_2O_5{\cdot}xH_2O$ nanobelts. The ion-induced synthesis of inorganic nanostructures has been successfully carried out in our previous work [26]. From the viewpoint of both chemistry and crystallography, owing to the chain-based slab structure, $V_2O_5{\cdot}xH_2O$ favors to form nanobelts along [010] direction or *b*-axis simulated by the chemical bonding theory of single crystal growth (Fig. 6c) [31]. While in the presence of $Mg^{2+}$, both top and bottom surfaces of nanobelts tend to adsorb $Mg^{2+}$ due to their terminated negative $O^{2-}$. During the growth process of nanobelts, once the amount of adsorbed $Mg^{2+}$ on the top or bottom surface is different, asymmetric strain emerges, and the so-called asymmetric strain [32] is realized by our designed cation-induced strategy. When $Mg^{2+}$-induced asymmetric strain energy is larger than the elasticity energy, straight nanobelts tend to

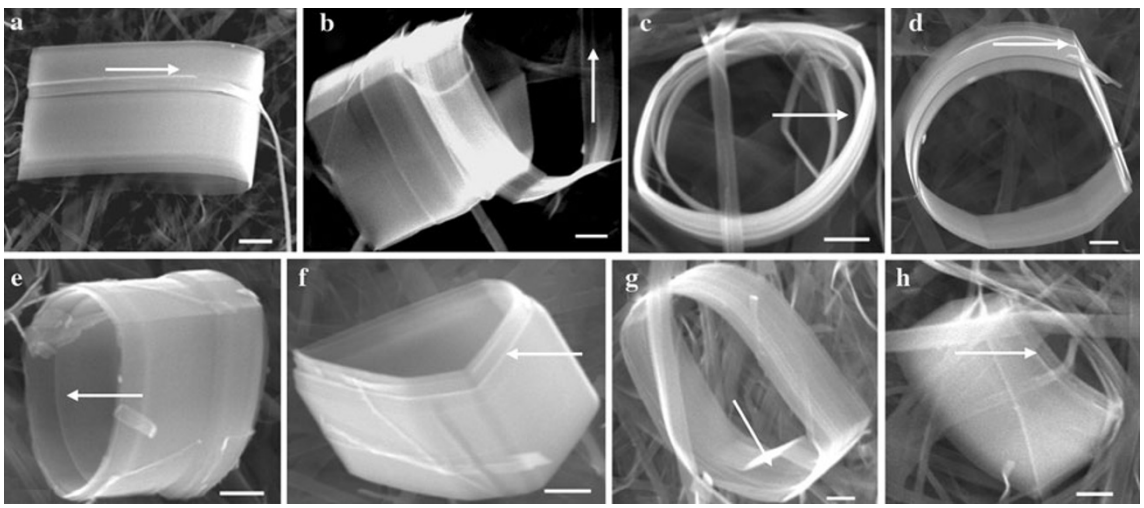


**Fig. 8** SEM images showing the direct evidences of coiling of nanoblets into $V_2O_5{\cdot}xH_2O$ nanorings and microloops. *Scale bars* correspond to 1 μm

coil into a circle structure. This structure is further stabilized by hydrogen bonding between these negative polar surfaces through bridged water molecules. The formation mechanism of the current nanorings is shown in Fig. 7 in detail. During the coiling process, the chemical environment such as the ion concentration and pH value may vary the asymmetric strain, which thus leads to formation of some trigonal and tetragonal morphologies (Fig. 3d, e, h,

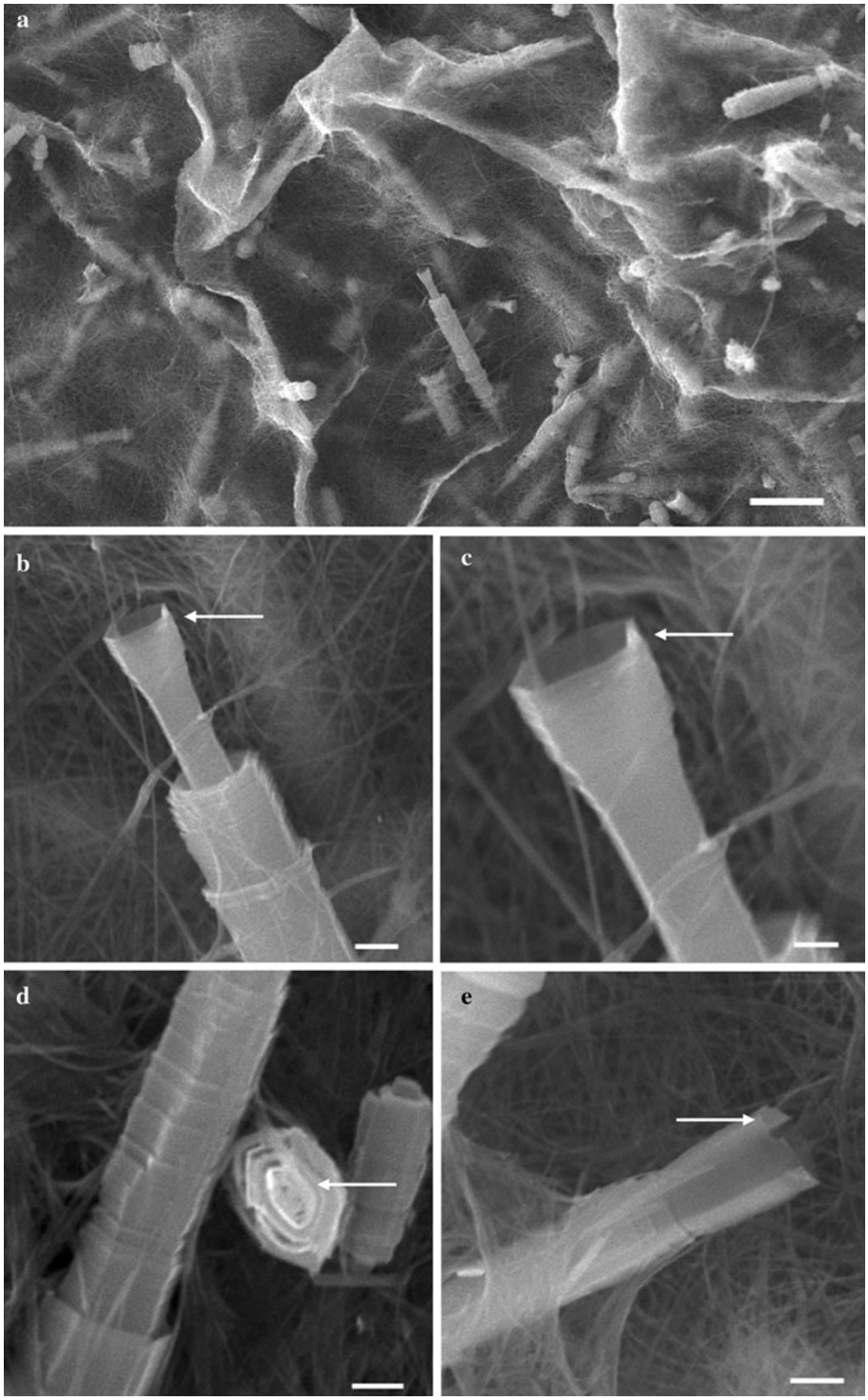


**Fig. 9** SEM images of $V_2O_5{\cdot}xH_2O$ microloops by coiling of nanobelts in the presence of $Zn^{2+}$. **a** Low-magnification SEM images of the samples. **b–e** High-magnification SEM images of the microtube-like loops showing the hollow cavity and coiled nanobelts. Scale bars correspond to 20 μm (**a**), 1 μm (**b–d**), and 500 nm (**e**)

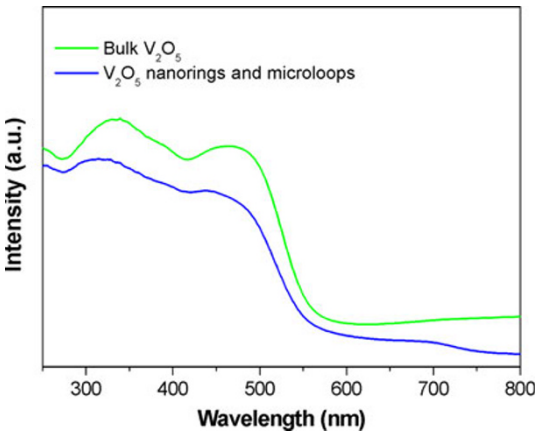


**Fig. 10** UV–Vis spectra of as-obtained $V_2O_5$ nanorings and microloops, and bulk $V_2O_5$ powders

i). In order to confirm the previous formation mechanism, we characterized the intermediate product at a shorter reaction time (10 h) by SEM (Fig. 8). Both ends and the screw coiling of $V_2O_5{\cdot}xH_2O$ nanobelts can be clearly seen. When we performed the synthesis without $Mg^{2+}$ in the reaction mixture while keeping other experimental conditions unchanged, only nanobelts can be obtained. Moreover, when $Zn^{2+}$ was added instead of $Mg^{2+}$, microloops were also obtained (Fig. 9), which confirmed our proposed cation-induced asymmetric strain formation mechanism.

To evaluate the optical properties of the obtained $V_2O_5$ nanorings and microloops, the UV–Vis spectrum of $V_2O_5$ are illustrated in Fig. 10. In comparison, we also characterized the UV–Vis spectrum of bulk $V_2O_5$ powders. As shown in the spectra, two major absorption bands for bulk $V_2O_5$ powders appear at about 330 and 470 nm, respectively. The absorption band above 450 nm corresponds to the band gap of $V_2O_5$. The absorption edge of $V_2O_5$ nanorings and microloops is blue-shifted compared to that of bulk $V_2O_5$ powders. The origin of the blue shift in the absorption edge is suggested to be the contribution of a quantum size effect in $V_2O_5$ nanorings and microloops [1, 7].

## Conclusions

In conclusion, single-crystalline $V_2O_5{\cdot}xH_2O$ nanorings and microloops were synthesized in the solution-phase system, by the cation-induced asymmetric strain on layered structure $V_2O_5{\cdot}xH_2O$ nanobelts. These as-synthesized $V_2O_5{\cdot}xH_2O$ nanorings and microloops may extend the application of $V_2O_5{\cdot}xH_2O$ in the area of gas sensors, actuators, and electric field-effect transistors. This work demonstrates that the novel nanoring structure, which has been observed previously only for polar surface dominated structure materials, is also available in other compounds without anion- and cation-terminated surfaces. Our proposed cation-induced strategy extends the existing formation mechanism of nanorings and can be applied to other materials.

**Acknowledgments** The financial support of the National Natural Science Foundation of China (Grant Nos. 50872016, 20973033) is acknowledged.



## References

1. J. Liu, D. Xue, Adv. Mater. **20**, 2622 (2008)
2. J. Liu, H. Xia, L. Lu, D. Xue, J. Mater. Chem. **20**, 1506 (2010)
3. J. Liu, F. Liu, K. Gao, J. Wu, D. Xue, J. Mater. Chem. **19**, 6073 (2009)
4. J. Liu, D. Xue, Mater. Res. Bull. **45**, 309 (2010)
5. S. Yin, B. Liu, P. Zhang, T. Morikawa, K. Yamanaka, T. Sato, J. Phys. Chem. C **112**, 12425 (2008)
6. J. Liu, D. Xue, J. Cryst. Growth **311**, 500 (2009)
7. C. Yan, D. Xue, Adv. Mater. **20**, 1055 (2008)
8. C. Yan, L. Nikolova, A. Dadvand, C. Harnagea, A. Sarkissian, D. Perepichka, D. Xue, F. Rosei, Adv. Mater. **22**, 1741 (2010)
9. J. Liu, D. Xue, Thin Solid Films **517**, 4814 (2009)
10. C. Yan, J. Liu, F. Liu, J. Wu, K. Gao, D. Xue, Nanoscale Res. Lett. **3**, 473 (2008)
11. S.L. Katar, A.B. Labiosa, A.E. Plaud, E.M. Vargas, L. Fonseca, B.R. Weiner, G. Morell, Nanoscale Res. Lett. **5**, 74 (2010)
12. F.L.S. Mello, L.O.O. Costa, E.P. Hernandez, A.M.D. De Farias, M.A. Fraga, Nanoscale Res. Lett. **5**, 1002 (2010)
13. V. Vega, V.M. Prida, M.H. Velez, E. Manova, P. Aranda, E.R. Hitzky, M. Vazquez, Nanoscale Res. Lett. **2**, 355 (2007)
14. S.A. Manafi, M.H. Amin, M.R. Rahimipour, E. Salahi, A. Kazemzadeh, Nanoscale Res. Lett. **4**, 296 (2009)
15. I. Alexandrou, E. Lioudakis, D. Delaportas, C.Z. Zhao, A. Othonos, Nanoscale Res. Lett. **4**, 635 (2009)
16. X.Y. Kong, Y. Ding, R.S. Yang, Z.L. Wang, Science **303**, 1348 (2004)
17. G.Z. Shen, D. Chen, J. Am. Chem. Soc. **128**, 11762 (2006)
18. D. Yu, J.Q. Wu, Q. Gu, H.K. Park, J. Am. Chem. Soc. **128**, 8148 (2006)
19. M. Nath, B.A. Parkinson, J. Am. Chem. Soc. **129**, 11302 (2007)
20. J. Liu, H. Xia, D. Xue, L. Lu, J. Am. Chem. Soc. **131**, 12086 (2009)
21. J. Muster, G.T. Kim, V. Krstic, J.G. Park, Y.W. Park, S. Roth, M. Burghard, Adv. Mater. **12**, 420 (2004)
22. G. Gu, M. Schmid, P.W. Chiu, A. Minett, J. Fraysse, G.T. Kim, S. Roth, M. Kozlov, E. Munoz, R.H. Baughman, Nat. Mater. **2**, 316 (2003)
23. S. Albonetti, G. Baldi, A. Barzanti, A.L. Costa, J.E. Mengou, F. Trifiro, A. Vaccari, Appl. Catal. A Gen. **325**, 309 (2007)
24. C.M. Leroy, M.F. Achard, O. Babot, N. Steunou, P. Masse, J. Livage, L. Binet, N. Brun, R. Backov, Chem. Mater. **19**, 3988 (2007)
25. N. Pinna, M. Willinger, K. Weiss, J. Urban, R. Schlogl, Nano Lett. **3**, 1131 (2003)
26. R. Tenne, Nature **431**, 640 (2004)
27. L.K. Elbaum, D.M. Newns, H. Zeng, V. Derycke, J.Z. Sun, R. Sandstrom, Nature **431**, 672 (2004)

28. V. Petkov, P.N. Trikalitis, E.S. Bozin, J.L. Billinge, T. Vogt, M.G. Kanatzidis, J. Am. Chem. Soc. **124**, 10157 (2002)
29. J. Livage, Chem. Mater. **3**, 578 (1991)
30. J.K. Bailey, G.A. Pozarnsky, M.L. Mecartney, J. Mater. Res. **7**, 2530 (1992)
31. X. Yan, D. Xue, Acta Mater. **55**, 5747 (2007)
32. O.G. Schmidt, K. Eberl, Nature **410**, 168 (2001)